Simulated annealing and object point processes : tools for analysis of spatial patterns

R. S. Stoica[1], P. Gregori[2] and J. Mateu[3]

University Jaume I
Campus Riu Sec, E-12071 Castellon, Spain

ABSTRACT
This paper introduces a three dimensional object point process - Bisous model - that we recommend to be used as a prior for three dimensional spatial pattern analysis. Maximization of likelihood or penalized-likelihood functions based on such a model requires global optimization techniques, such as the simulated annealing algorithm. Theoretical properties of the model are discussed and the convergence of the proposed optimization method is proved. Finally, a simulation study is presented.

2000 Mathematics Subject Classification: 60G55, 60J22, 62M30, 62M40.
Keywords and Phrases: Bisous model, object point process, marked point process, three dimensional spatial patterns, Markov chain Monte Carlo simulation, simulated annealing, cooling schedules, stochastic optimization.
Note: The work of the first author was supported by the grant SB2001-0130 of Spanish Ministery of Education, Culture and Sport.

1 Introduction

Since the end of the last century, the flood of data is an obvious un-stoppable reality for all the scientifical fields. Satellites or astronomical telescopes, particle accelerators or microscopes, under the developement of the technology, provide us continuously with data coming from all the sides of our universe, at macro and micro scales. The main motivation of provocating such a "meteorological" phenomenon is that using appropriate tools (*i.e.* mathematical models), we can retrieve from the provided data the useful information allowing us to answer at the questions arising from the corresponding domains.

Let us consider the data we dispose having two major components : a

[1]stoica@guest.uji.es
[2]gregori@mat.uji.es
[3]mateu@mat.uji.es

location inside a defined region, and a vector of numerical values asigned to this location. Remotely sensed images or astronomical catalogs of galaxies are good examples of such data. The information we may wish to extract can be represented by spatial patterns like hydrographic networks and maps of different crop fields in cartography, or filamentary structure and walls formed by galaxies in astronomy.

Stochastic modelling is one possible way of formulating solutions for such problems. Let $\mathbf{x}$ be the observed data, and $\mathbf{y}$ the pattern we look for, under the hypothesis that $\mathbf{y}$ is the realization of a random process. The configuration $\hat{\mathbf{y}}$ that maximizes the posterior law $p(\mathbf{y}|\mathbf{x})$ is the *Maximum A Posteriori* (MAP) estimator of the desired solution. Following the Bayes' rule, we write

$$\hat{\mathbf{y}} = \arg\max_{\mathbf{y}} p(\mathbf{x}|\mathbf{y})p(\mathbf{y}) \tag{1}$$

with $p(\mathbf{x}|\mathbf{y})$ and $p(\mathbf{y})$ the conditional and the prior probability densities respectively. The likelihood defined as the joint distribution of the data given the pattern is not always accessible. Hence, the estimator given by (1) does not represent the MAP, but it is the maximum of the likelihood $p(\mathbf{y})$ penalized by the external field $p(\mathbf{x}|\mathbf{y})$.

There are three necessary ingredients for building a spatial pattern analysis tool based on stochastic modelling : the conditional probability depending on the data, the prior giving a general aspect of the solution, and finally an optimization method.

This paper is dedicated to the last two points mentioned above, *i.e.* the prior modelling for spatial patterns using marked point processes, and the optimization technique based on the simulated annealing algorithm.

Modelling prior distributions using marked point processes was introduced in pattern analysis problems by statisticians involved in image processing [1, 10, 16, 25, 29, 30, 31]. One of their main contribution consists of the natural modelling of the image as a collection of objects rather than a set of numerical values. Following these directions, solutions were brought to questions arising from remotely sensed image processing by developing models for complex geometrical shapes such that hydrographical and road networks or building configurations [3, 15, 24, 34].

Despite the very good results obtained on two dimensional problems very few work was done in analysing three dimensional patterns using marked point processes.

The first part of the paper tries to fill a real need, proposing a new marked point process - the Bisous model - to be used as a basis for constructing prior models in spatial pattern analysis. The introduced model is able to simulate

complex three dimensional spatial patterns. The patterns are supposed to be random configurations of simple objects like segments, polygons or polyhedra. The local interactions exhibited by these objects allow to form complex geometrical structures like filaments, surfaces (curved plates) and clusters. Theoretical properties of the model such as Markovianity and local stability are also discussed.

The second part of the paper is dedicated to the construction of a simulated annealing algorithm. This method is a global optimization technique borrowed from statistical physics [13]. The algorithm works by sampling the probability law of interest under the control of an extra parameter, the temperature. If the temperature is cooled slowly enough, the algorithm converges towards configurations maximizing the probability law of interest, avoiding the local minima. Obviously, the main ingredients needed when implementing such a method are a sampling method for the probability law to simulate and a cooling schedule driving the temperature. When discrete models defined on a finite state space are used, the convergence of such an algorithm is proved in [4, 9]. The case of marked point processes simulated using a spatial birth-and-death dynamics is tackled by [16]. For the simulated annealing method we propose, a tailored to the model Metropolis-Hastings dynamics is used , and a proof of the convergence of the algorithm is given, allowing the derivation of a cooling schedule equivalent to the one presented by [4, 9].

Finally, simulations are shown and discussed and conclusion and perspectives are depicted.

2 Object point processes : preliminaries and notations

Let ν be the Lebesgue measure in $\mathbb{R}^3$, K a compact subset of $\mathbb{R}^3$ such that $0 < \nu(K) < \infty$, and $(K, \mathcal{B}_K, \nu)$ the natural restriction to K of the measure space $(\mathbb{R}^3, \mathcal{B}, \nu)$.

For $n \in \mathbb{N}_0$, let K_n be the set of all unordered configurations $\mathbf{x} = \{k_1, k_2, \ldots, k_n\}$ that consist of n not necessarily distinct points $k_i \in K$. K_0 is the empty configuration. We consider the configuration space given by $\Omega_K = \cup_{n=0}^{\infty} K_n$ equipped with the $\sigma-$algebra $\mathcal{F}_K$ generated by the mappings $\{k_1, \ldots, k_n\} \to \sum_{i=1}^{n} \mathbf{1}\{k_i \in B\}$ that count the number of points in Borel sets $B \in \mathcal{B}_K$. Hence, a point process on K is a measurable map from a probability space into $(\Omega_K, \mathcal{F}_K)$.

To each point, different characteristics may be attached by means of a

marked point process. Let us consider a point process on $K \times M$ as the random sequence $\mathbf{y} = \{(k_i, m_i)\}_{i=1}^{n}$ where $k_i \in K$ is the location of the point and $m_i \in M$ its attached mark. Furthermore, M the mark space is equiped with $\mathcal{M}$ the corresponding $\sigma-$ algebra and the probability measure ν_M. The point process on $K \times M$ is called a marked point process, if the distribution of the locations only is point process on K [17]. A marked point process with marks designing characteristics of objects, is commonly named an *object point process*.

Several types of objects may be considered. Let $\mathcal{T}$ be the set of types of objects. For each $t \in \mathcal{T}$, we construct the probability space $(M_t, \mathcal{M}_t, \nu_t)$ with M_t the parameter space for objects of type t, $\mathcal{M}_t$ the induced $\sigma-$algebra and ν_t a pre-defined probability measure.

Let $(M, \mathcal{M}, \nu_M)$ be the shape space, a probability space with state space M and induced $\sigma-$algebra $\mathcal{M}$ given by the following disjoint unions, respectively :

$$M = \cup_{t\in\mathcal{T}} M_t, \quad \mathcal{M} = \cup_{t\in\mathcal{T}} \mathcal{M}_t.$$

Here, the probability measure ν_M is given by

$$\nu_M(B) = \sum_{t\in\mathcal{T}} \alpha_t \nu_t(B \cap M_t) \qquad B \in \mathcal{M} \tag{2}$$

with $(\alpha_t)_{t\in\mathcal{T}}$ an arbitrary nonnegative sequence holding $\sum_{t\in\mathcal{T}} \alpha_t = 1$.

There are several ways of defining the measure ν_M. The way we have chosen to do it, illustrates theoretically a manner of modelling a scene with an infinite typology of objects.

Thus, we consider a configuration of objects as a finite set of marked points. Similarly, as for the un-marked case, for $n \in \mathbb{N}_0$, Ξ_n is the set of all (unordered configurations) $\mathbf{y} = \{y_1, \ldots, y_n\}$ consisting of not necesssarily distinct marked points $y_i \in K \times M$. Ξ_0 is the configuration with no objects. The configuration space can be written as $\Omega = \cup_{n=0}^{\infty} \Xi_n$ and equiped with the $\sigma-$algebra $\mathcal{F}$ defined by the mapping that counts the number of marked points in Borel sets $A \subseteq K \times M$. An object point process is a measurable map from a probability space into $(\Omega, \mathcal{F})$.

At our knowledge the simplest object point process is the Poisson object point process of probability measure

$$\begin{aligned} \mu(F) \quad = \quad & \sum_{n=0}^{\infty} \frac{e^{-\nu(K)}}{n!} \int_{K\times M} \cdots \int_{K\times M} \mathbf{1}_F\{(k_1, m_1) \ldots, (k_n, m_n)\} \\ & \times d\nu(k_1) \cdots d\nu(k_n) d\nu_M(m_1) \ldots d\nu_M(m_n) \end{aligned}$$

for all $F \in \mathcal{F}$. According to a Poissson law of intensity $\nu(K)$, μ distributes the objects uniformly in K, with their corresponding shapes chosen independently according to ν_M.

When interactions between objects have to be taken into account, more complicated models are needed. They can be constructed by specifying a Radon-Nikodým derivative $p(\mathbf{y})$ with respect to μ. The negative logarithm $U(\mathbf{y}) = -\log p(\mathbf{y})$ is known by the physicists as the total Gibbs energy of a system of particles $\mathbf{y}$.

For any specified object point process, the integrability of its unormalized probability density with respect to a Poisson object process is ensured by the Ruelle's condition [32], that requires

$$\frac{p(\mathbf{y})}{p(\emptyset)} \leq \Lambda^{n(\mathbf{y})} \tag{3}$$

holds for a finite constant $\Lambda > 0$ and any $\mathbf{y} \in \Omega$. In this case the process is called *stable*.

An even stronger condition than (3) is defined as follows

$$\lambda(\xi; \mathbf{y}) = \frac{p(\mathbf{y} \cup \{\xi\})}{p(\mathbf{y})} \leq \Lambda \tag{4}$$

with $\Lambda > 0$ finite, for all $\mathbf{y} \in \Omega$ and $\xi \in K \times M$. $\lambda(\xi; \mathbf{y})$ is called the Papangelou conditional intensity.

If condition (4) is satisfied the model is said to be *locally stable*. This condition is also needed to prove the convergence properties of the Monte Carlo dynamics simulating the model.

3 Bisous model : a general model for spatial patterns

The main hypothesis along this paper is that a spatial pattern is the realization of an object point process - called *Bisous model*. In words, we think of a pattern as a random collection of objects that interact. For instance, segments that connect and have close orientations may form filaments (lines). In the same way, polygons or polyhedra that group together under similar conditions may give birth to surfaces (plans) or volumes (clusters), respectively.

In this section we first present some objects and interactions between them, that are able to form patterns like the ones we have mentioned. Next, the probability density corresponding to our model, the Bisous model, is introduced. Some analytical properties of the proposed marked process are finally discussed.

3.1 Definition of objects

The objects we consider to form patterns with, are described by their random location in K and their corresponding mark, here a three dimensional random orientation vector ω given by its parameters $\omega = \phi(\theta, \eta)$ uniformly distributed on $M = [0, 2\pi) \times [-1, 1]$ such that

$$\omega = (\sqrt{(1-\eta^2)}\cos(\theta), \sqrt{(1-\eta^2)}\sin(\theta), \eta).$$

In order to create patterns, objects need to group together. Hence an attraction region is induced around an object by a finite number q of rigid extemity points $\{e_u, 1 \leq u \leq q\}$.

Definition 1. *The attraction region $a(y)$ around an object $y = (k, \omega)$ is defined by the disjoint union $a(y) = \bigcup_{u=1}^{q} b(e_u, r_a)$, where $b(e_u, r_a)$ is the ball of fixed radius r_a centered in e_u.*

In the following, we give some definitions of interactions that help us to favour or to penalize configurations of objects forming different kind of patterns.

The extremity points of an object are indexed.

Definition 2. *The attraction rule $\mathcal{C}$ for two objects y_i and y_j is the set of pairs of indices corresponding to the extremity points allowed to form an attraction interaction.*

For instance, attraction may be allowed only if extremity points with even indexes are closer than r_a.

Definition 3. *Two objects $y_i = (k_i, \omega_i)$ and $y_j = (k_j, \omega_j)$ are attracting each other, and we write $y_i \sim_a y_j$, if the set $\{(u, v) : 1 \leq u, v \leq q, d(e_u(y_i), e_v(y_j)) \leq r_a\}$ contains only one element that verifies the condition $\mathcal{C}$.*

Definition 4. *Two objects $y_i = (k_i, \omega_i)$ and $y_j = (k_j, \omega_j)$ exhibit a hard-repulsion, and we write $y_i \sim_h y_j$, if $d(k_i, k_j) \leq 2r_h$. The same objects exhibit a soft-repulsion $y_i \sim_r y_j$, if $2r_h < d(k_i, k_j) \leq r_s = 2r_h + r_\epsilon$. Here we consider $0 < r_\epsilon < r_h < r_s$.*

Definition 5. *Two objects $y_i = (k_i, \omega_i)$ and $y_j = (k_j, \omega_j)$ are aligned, and we write $y_i \sim_\parallel y_j$, if*

$$\omega_i \cdot \omega_j \geq 1 - \tau$$

where $\tau \in (0, 1)$ is a predefined curvature parameter and $\cdot$ designes the scalar product between the two orientation vectors.

Definition 6. *Two objects $y_i = (k_i, \omega_i)$ and $y_j = (k_j, \omega_j)$ are connected $y_i \sim_s y_j$ if they attract each other $y_i \sim_a y_j$ and if the following conditions are simultaneously fulfilled*

$$y_i \not\sim_h y_j$$
$$y_i \sim_{\parallel} y_j$$

Definition 7. *Let $\mathcal{R}$ be the set of all possible interactions between objects constructed on $K \times M$ that are pairwise, local (distance based), symmetric and induce measurable mappings on $\mathcal{F}$.*

All the relations defined previously are symmetric and reflexive, with the exception of the attraction and the connectivity, which are just symmetric. It can be checked that $\sim_h, \sim_r, \sim_a, \sim_s$ belong to $\mathcal{R}$. The interaction $\sim_{\parallel}$ does not belong to $\mathcal{R}$ since it is not local.

Definition 8. *An object is said to be $s-$connected if it is connected at exactly s from its q extremity points. If $s = 0$, the object is called free.*

Definition 9. *Two objects are of the same type if they are defined on the same parameter space, have the same number of extremity points q and follow the same attraction rule $\mathcal{C}$.*

In this work, a pattern is a configuration of objects of the same type.

Example 1. Line pattern. *In Figure 1 an object able to construct a filamentary network is showed. The generating element is a segment of fixed length $2(r + r_a)$, centered at the origin, with $q = 2$ extremity points*

$$e_u = (0, 0, (r + r_a) \sin \frac{(2u-1)\pi}{2}), \quad 1 \leq u \leq q.$$

and orientation vector $\omega = (0, 0, 1)$.

The repulsion radii are $r_h = r$ and $r_\epsilon = 4r_a$ respectively. In this case, the attraction rule $\mathcal{C}$ is defined such that two objects y_i and y_j attract each other only by means of extremity points $e_u(y_i)$ and $e_v(y_j)$ having different indices $u \neq v$. Hence, the attraction rule is $\mathcal{C} = \{(1, 2), (2, 1)\}$.

Clearly, such a segment with random location and random orientation can be obtained by means of a translation combined with two rotations applied to the segment [11].

Example 2. Planar pattern. *In Figure 2, the generating element for a planar pattern is considered as the hexagone centered at the origin, with the orientation vector $\omega = (0, 0, 1)$ and $q = 6$ extremity points given by*

$$e_u = ((r + r_a) \cos \frac{(2u-1)\pi}{6}, (r + r_a) \sin \frac{(2u-1)\pi}{6}, 0), \quad 1 \leq u \leq q.$$

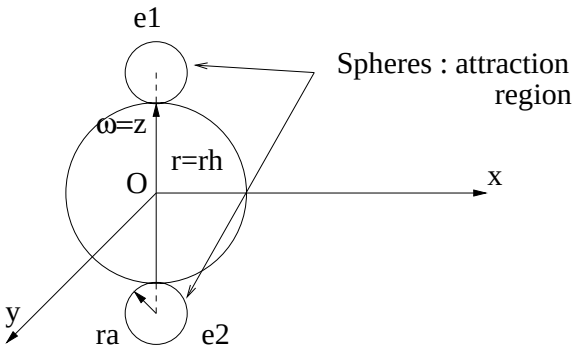

Figure 1: Generating element for a line pattern

The repulsion regions are defined exactly in the same way as in the previous example. In this case, the rule $\mathcal{C}$ is defined such that $|u - v| = 3$ for the pair of extremity points $(e_u(y_i), e_v(y_j))$ fulfilling the attraction condition. Hence, the attraction rule is $\mathcal{C} = \{(1,4),(4,1),(2,5),(5,2),(3,6),(6,3)\}$.

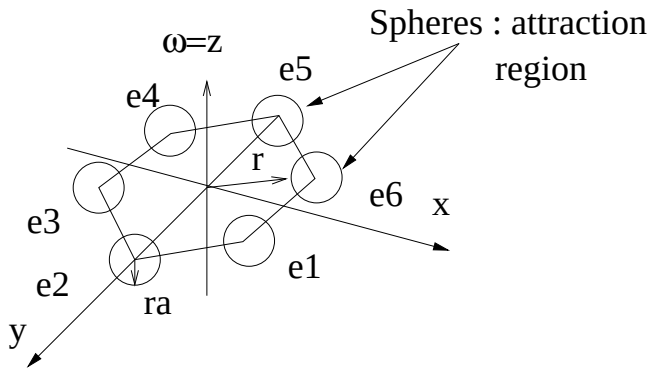

Figure 2: Generating element for a planar pattern

Example 3. Cluster pattern. *In Figure 3 we show as generating element for a clustered pattern the cuboctahedron having its center at the origin, the orientation vector $\omega = (0,0,1)$ and $q = 12$ extremity points such that*

$$e_u = ((r+r_a)\cos(\alpha_u+\beta_u), (r+r_a)\sin(\alpha_u+\beta_u), (r+r_a)\sin(\beta_u/2)) \quad 1 \leq q \leq 12,$$

where $\alpha_u = \frac{\pi}{4}(2u-1)$ and $\beta_u = \frac{\pi}{2}\left[\frac{u-5}{4}\right]$.

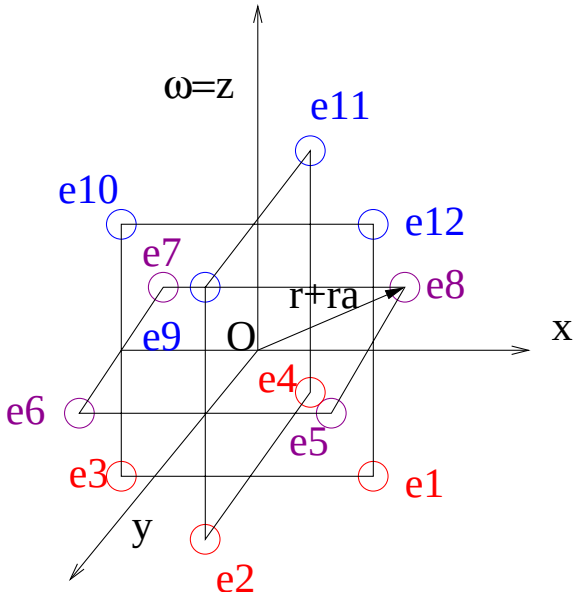

Figure 3: Generating element for a cluster pattern

Around the object, rejection regions are defined exactly like in the previous cases. Here, the rule $\mathcal{C}$ is defined such that the attraction between two objects y_i and y_j occurs by means of the extremity points $e_u(y_i)$ and $e_v(y_j)$ such that u and v are opposite indices. By opposite indices (u, v) we design the following pairs of authorized attracting indices $(1, 10)$, $(2, 11)$, $(3, 12)$, $(4, 9)$, $(5, 7)$, $(6, 8)$ and their symmetrics respectively.

In our examples we gave attraction rules between objects of the same type. Depending on the kind of applications, we can think of more complex mechanisms of attraction or any other interaction exhibited by pairs of objects not being of the same type.

3.2 Construction of the probability density

Lemma 1. *The mappings that count, in a configuration of objects of the same type $\mathbf{y} \in \Omega$, the number of $s-$connected objects n_s for $s = 0, 1, 2, \ldots, q$ are measurable with respect to $\mathcal{F}$.*

The proof is an adaptation of ([18], Lemma 1).

Proof: In the following we proof the measurability of the mapping counting

the number of free objects n_0. The measurability for all the other mappings holds by similar arguments.

By ([27], Section 3.1) we need to prove the Borel measurability of the symmetric function

$$f(y_1,\ldots,y_n):(K\times M)^n\to\sum_{i=1}^{n}\mathbf{1}\{y_i \quad \text{is free}\}$$

for all $n\in\mathbb{N}_0$.

For fixed $i\neq j\in\{1,\ldots,n\}$ let us define f_{ij} such that

$$\begin{aligned} f_{ij}(y_1,\ldots,y_n) \quad = \quad & \mathbf{1}\{y_i \not\sim_a y_j\}+\mathbf{1}\{y_i\sim_a y_j\}\mathbf{1}\{y_i\sim_h y_j\}+\\ & \mathbf{1}\{y_i\sim_a y_j\}\mathbf{1}\{y_i\not\sim_h y_j\}\mathbf{1}\{y_i\not\sim_{\|} y_j\}\end{aligned}$$

The function f_{ij} is Borel measurable as a mapping on $(K\times M)^n$. Clearly, the function

$$\mathbf{1}\{y_i \quad \text{is free}\}=\prod_{i\neq j}f_{ij}(y_1,\ldots,y_n)$$

is also Borel measurable and so the sum of these functions over i. □

For a configuration of objects of the same type $\mathbf{y}=\{y_1,\ldots,y_n\}$, $i=1,\ldots,n=n(\mathbf{y})$ the *Bisous model* is defined by the following probability density with respect to the reference Poisson object process

$$p(\mathbf{y})=p(\emptyset)\left[\prod_{s=0}^{q}\gamma_s^{n_s(\mathbf{y})}\right]\prod_{\kappa\in\Gamma\subset\mathcal{R}}\gamma_\kappa^{n_\kappa(\mathbf{y})} \tag{5}$$

where $\gamma_s>0,\gamma_\kappa\in[0,1]$ are the model parameters, $p(\emptyset)$ is the normalizing constant and Γ is the set that contains the pairwise interactions from $\mathcal{R}$ taken in account to build the pattern $\mathbf{y}$. If $\gamma_k=0$ the interaction $\sim_\kappa$ is said to be hard-core (we use the convention $0^0=1$). For each s and κ the sufficient statistics $n_s(\mathbf{y})$ and $n_\kappa(\mathbf{y})$ represent respectively the number of $s-$ connected objects and the number of pairs of objects exhibiting the interaction κ in a configuration $\mathbf{y}$.

Lemma 2. *The Bisous model specified by (5) is locally stable.*

Proof: K is a compact subset of $\mathbb{R}^3$ such that $0<\nu(K)<\infty$.

If $\sim_h\in\Gamma$ and it is a hard-core interaction (*i.e.* $\gamma_h=0$), there is a maximum of objects $n_{\max}$ that can be contained in K.

Hence, the conditional intensity is bounded by :

$$\lambda(\zeta; \mathbf{y}) \leq \prod_{s=0}^{q} \max\{\gamma_s, \gamma_s^{-1}\}^{n_{\max}} = \Lambda$$

Even if Γ contains no such hard-core interaction, the model is still locally stable. We notice that the maximum number of not connected objects, that can connect another object via only one extremity point, is 12 - the kissing number. The bound for the conditional intensity becomes :

$$\Lambda = \prod_{s=0}^{q} \max\{\gamma_s, \gamma_s^{-1}\}^{12} \tag{6}$$

As connectivity requires alignment between the interacting objects, we can find smaller bounds for Λ depending on the allowed curvature τ. □

Theorem 1. *The unnormalized density (5) of the Bisous model specifies a well-defined object point process.*

Proof: The $(\Omega, \mathcal{F})-$ measurability of the Bisous model follows from the definition of $\mathcal{R}$ and Lemma 1. The local stability property implies Ruelle's stability (3) that guarantees the integrability of (5). □

The Bisous model and the presented results are clearly the three dimensional extension and the generalization with respect the considered pairwise interactions of the Candy model [18]. Like its predecesor, the Bisous model exhibits symmetric, pairwise interactions that are local. The $s-$connectivity is also symmetric and has a range of $2(r_h + r_a)$. By these arguments and supposing the empty set and singletons cliques, we infer that the Bisous model belongs to the class of (Ripley-Kelly) Markov point processes [28].

4 Simulated annealing algorithm

In many practical applications like pattern recognition, image analysis or particle physics, there is a lot of interest in maximizing probability laws $p(\mathbf{y})$ given by (5).

The commonly adopted solution is the simulated annealing method [4, 13], a global optimization method that iteratively samples from

$$p_n(\mathbf{y}) \propto [p(\mathbf{y})]^{\frac{1}{T_n}} \tag{7}$$

with T_n the temperature parameter. When $T_n \to 0$ slowly enough, the algorithm generates a Markov chain which converges in distribution towards the uniform distribution over the set of configurations maximizing $p(\mathbf{y})$.

In the following we present the two ingredients needed for implementing such an optimization technique, a sampling method and a cooling schedule.

4.1 Choices for sampling the Bisous model

Sampling from densities of marked point processes requires of Monte Carlo techniques, since their normalizing constant is analytically untractable.

The idea behind these methods is to construct a transition kernel $P_n(\mathbf{y}, A)$ of invariant distribution

$$\pi_n(A) = \int_A p_n(\mathbf{y})\mu(d\mathbf{y}).$$

to iteratively simulate a Markov chain. If the simulated chain is aperiodic and $\phi-$irreducible, then the invariant distribution is unique and it is also the equilibrium distribution of the chain.

Two other very important properties are needed when constructing a Markov chain, the Harris recurrence and the geometric ergodicity. The first property ensures the convergence to the equilibrium distribution independently of the initial conditions, whereas the geometric ergodicity often implies a Central Limit Theorem, allowing the approximation of integrals

$$\mathcal{I} = \int g(\mathbf{y})\pi_n(d\mathbf{y})$$

with g a π_n-integrable function, by sums of the form

$$\widehat{\mathcal{I}} = \frac{1}{k}\sum_{i=1}^{k} g(Y_i)$$

where the Y_i are sampled from π_n. For a deeper look on these properties we suggest [6, 36] and the excellent monograph [22].

Among the existing sampling methods, several choices may be depicted such as spatial birth-and-death processes, reversible jumps dynamics, or the much more recent exact simulation methods [5, 6, 7, 12, 17, 19, 26].

The Bisous model (5) exhibits a high local stability constant (6). Furthermore the model is nor monotonic neither anti-monotonic in the sense of [12]. This discards from the candidate samplers, the methods based on

spatial birth-and-death processes and the exact simulation algorithms associated to it, like coupling from the past or clan of ancestors. Theoretically these methods work perfectly, but in practice such a choice impose to simulate the model within a limited range of parameters.

We gave our preference to the Metropolis-Hastings dynamics [5, 6], method that is a special case of the reversible jump Monte Carlo framework in [7].

The transition kernel built to explore the state space uses three types of transition :

• birth - with probability p_b a new object ζ sampled from the birth proposal $b(\mathbf{y}, \zeta)$ is proposed to be added to the present configuration $\mathbf{y}$; the new configuration $\mathbf{y}' = \mathbf{y} \cup \{\zeta\}$ is accepted with probability

$$\min\left\{1, \frac{p_d}{p_b}\frac{d(\mathbf{y}\cup\{\zeta\},\zeta)}{b(\mathbf{y},\zeta)}\frac{p_n(\mathbf{y}\cup\{\zeta\})}{p_n(\mathbf{y})}\right\} \tag{8}$$

• death - with probability p_d an object ζ from the current configuration $\mathbf{y}$ is chosen according to the death proposal $d(\mathbf{y}, \zeta)$; the probability of accepting the new configuration $\mathbf{y}' = \mathbf{y} \setminus \{\zeta\}$ is computed reversing the ratio (8)
• change - with probability p_c choose an object ξ in the configuration $\mathbf{y}$ according to probability $q(\mathbf{y}, \xi)$; using the proposal $c(\mathbf{y}, \xi, \zeta)$, accept the new configuration $\mathbf{y}' = \mathbf{y} \setminus \{\xi\} \cup \{\zeta\}$ with probability

$$\min\left\{1, \frac{q(\mathbf{y}\setminus\{\xi\}\cup\{\zeta\},\zeta)}{q(\mathbf{y},\xi)}\frac{c(\mathbf{y}\setminus\{\xi\}\cup\{\zeta\},\zeta,\xi)}{c(\mathbf{y},\xi,\zeta)}\frac{p_n(\mathbf{y}\setminus\{\xi\}\cup\{\zeta\})}{p_n(\mathbf{y})}\right\} \tag{9}$$

Usually, uniform proposals $c(\mathbf{y}, \xi, \zeta)$ are used. The old object ξ is changed into the new one ζ, by modifying its initial parameters in a local neighborhood. For the proposed transition kernel, we have constructed three change moves that act respectively on the centre and the mark of a considered object.

The uniform choices $b(\mathbf{y}, \zeta) = \frac{1}{\nu(K)}$ and $d(\mathbf{y}, \zeta) = \frac{1}{n(\mathbf{y})}$ are commonly adopted for their simplicity and because they guarantee the irreducibility, the Harris recurrence and the geometric ergodicity of the simulated chain. For the probabilities p_b,p_d and p_c, all the convergence properties are preserved as long as $p_b + p_d + p_c \leq 1$.

Still, when the model to simulate exhibits complicated interactions, such an update mechanism made of uniform birth and death proposals, may be very slow in practice. Here, we adopt the strategy proposed for simulating the Candy model, that recommends the use of adapted moves that help the model [18].

In our case, the adapted move we consider is a non-uniform mixture for the birth proposal

$$b(\mathbf{y},\zeta) = \frac{p_1}{\nu(K)} + p_2 b_a(\mathbf{y},\zeta)$$

with $p_1 + p_2 = 1$ and $b_a(\mathbf{y},\zeta)$ a probability density proposing attracting and well aligned objects.

Simillary to the two-dimensional case presented in [18], the expression of $b_a(\mathbf{y},\zeta)$ is given by

$$b_a(\mathbf{y},\zeta) = \frac{1}{n(A(\mathbf{y}))} \sum_{y \in A(\mathbf{y})} \tilde{b}(y,\zeta)$$

where $A(\mathbf{y})$ is the set of objects in the configuration $\mathbf{y}$ which are not $q-$connected. Hence, the objects contained in the set A have at least an extremity point able to make connection with another object. After choosing uniformly an object y from the set $A(\mathbf{y})$, a new object $\zeta = (k_\zeta, \omega_\zeta)$ of parameters (k, θ, η) is proposed to be added using the density

$$\tilde{b}(y,\zeta) = f(k|y)g(\theta)h(\eta) \tag{10}$$

The uniform updates are used in (10) as follows :

$$f(k|y) = \frac{\mathbf{1}\{k \in \tilde{a}(y)\}}{\nu(\tilde{a}(y) \cap K)} \tag{11}$$

$$g(\theta) = 1 \tag{12}$$

$$h(\eta) = \frac{2}{\tau}\mathbf{1}\{\eta \in (1-\tau, 1)\} \tag{13}$$

where $\tilde{a}(y) = \bigcup_{u=1}^{\tilde{q}} b(e_u(y), r_a)$ is the region made of the union of attraction balls of y which are not containing the extremity of any other attracting object in the configuration $\mathbf{y}$. Clearly, using θ and η, the direction vector ω_ζ is obtained by means of one translation and two rotations such that the alignment conditions are satisfied with respect ω_y. By means of a translation respecting the corresponding attraction rule $\mathcal{C}$, the point k becomes the centre of the new object k_ζ.

This birth proposal helps the model in proposing configurations with connected objects much more often than the uniform proposal only.

Following [18], the use of such an adapted transition kernel is guaranteed with all the mentioned convergence properties, provided that

$$\sup_{\zeta \in \Omega, n(\mathbf{y})=n} \frac{d(\mathbf{y} \cup \{\zeta\}, \zeta)}{b(\mathbf{y},\zeta)} \to 0$$

when $n \to \infty$.

4.2 Cooling schedule

The second key element of a simulated annealing algorithm is the cooling schedule. For instance, in the case of finite state spaces, a logarithmic cooling schedule is proved to be optimal when used with the Gibbs sampler [4]. The same result is obtained by [9] when a different Markov chain is used.

The case of marked point process is more delicate since the state space is infinite. The proof of the existence of simulated annealing based on a spatial birth-and-death sampler is given in [16].

In this section, we prove the convergence of a simulating annealing algorithm based on the Metropolis-Hastings previously introduced.

Theorem 2. *Let $\Omega_\star$ be the set of configurations maximizing $p(\mathbf{y})$ given by (5) and assume $\mu(\Omega_\star) > 0$. Let T_n be a sequence such that $\lim_{n\to\infty} T_n = 0$ and consider the probability densities p_n given by (7) with respect to reference measure μ on Ω. Then the sequence p_n converges in total variation to the uniform distribution on $\Omega_\star$.*

Moreover, the sequence of probability densities satisfies:

$$\sum_{n=1}^{\infty} \| \pi_n - \pi_{n+1} \| < \infty \tag{14}$$

where $\| \cdot \|$ stands for the total variation distance.

Proof: See the proof in ([16], Section 6.1, Lemma 9). □

The Dobrushin's coefficient is a useful tool for proving the convergence of simulated annealing algorithms [4, 9, 16].

Definition 10. *For a transition kernel $Q(\cdot,\cdot)$ on $(\Omega, \mathcal{F})$, Dobrushin's contraction coefficient $c(Q)$ is defined by*

$$c(Q) = \sup_{\mathbf{x},\mathbf{y}\in\Omega} \| Q(\mathbf{x},\cdot) - Q(\mathbf{y},\cdot) \| \tag{15}$$

Theorem 3. *Let $(Y_n)_{n\geq 0}$ be a non-stationary Markov process on the measurable space $(\Omega, \mathcal{F})$, defined by the transition kernels*

$$Q_n(\mathbf{y}, F) = P_n^\delta(\mathbf{y}, F)$$

where P_n^δ is the application $\delta-$times of the transtion kernel P_n defined by the Metropolis-Hastings updates (8) and (9). Assume also, that conditions

$$\sum_{n=1}^{\infty} \| \pi_n - \pi_{n+1} \| < \infty \tag{16}$$

and

$$\lim_{n\to\infty} c(Q_{n_0,n}) = 0 \tag{17}$$

hold for all $n_0 \geq 0$ *and transition probabilities* $Q_{n_0,n}(\mathbf{y}, F) = \mathbb{P}(Y_n \in F | Y_{n_0} = \mathbf{y})$. *Then the limit of the sequence* $\lim_{n\to\infty} \pi_n = \pi_\infty$ *exists and also* $\lim_{n\to\infty} \pi_0 Q_{0,n} = \pi_\infty$ *in total variation, for any initial distribution* π_0.

Proof: Since π_n is the invariant measure of $P_n(\mathbf{y}, F)$ by construction, it is also the invariant measure for $Q_n(\mathbf{y}, F)$. The condition (16) clearly is provided by Theorem 2. Let us suppose the condition (17) verified. Hence, by ([16], Section 3.2, Theorem 4) the proof is completed. □

We still have to show that the Dobrushin's condition (17) is fulfilled.

Theorem 4. *Let* $Q_n(\mathbf{y}, F) = P_n^\delta(\mathbf{y}, F)$ *be the transition kernel given in Theorem 3. If the step* δ *is a finite integer, such that* $n(\mathbf{y}) \leq \delta$ *for all the configurations of objects* $\mathbf{y} \in \Omega$, *then the Dobrushin's condition (17) holds.*

Proof: By the properties of Dobrushin's coefficient and by the arguments in ([16], Section 3.2, Lemma 5) the proof is completed if

$$c(Q_n) \leq 1 - \frac{1}{n} \tag{18}$$

Let us compute $P_n^\delta(\mathbf{y}, \Xi_0)$ the probability of going from any $\mathbf{y} \in \Omega$ to the empty configuration in δ steps. One way to do it is proposing and accepting $n(\mathbf{y})$ death moves, and then staying in the empty configuration another $\delta - n(\mathbf{y})$ steps. By means of Kolmogorov-Chapmann equations, we can write the following inequality

$$P_n^\delta(\mathbf{y}, \Xi_0) \geq P_n^{n(\mathbf{y})}(\mathbf{y}, \Xi_0) P_n^{\delta - n(\mathbf{y})}(\emptyset, \Xi_0) \geq (p_b \Delta_n)^\delta \tag{19}$$

with the term Δ_n given by

$$\Delta_n = \frac{1}{\nu(K)\Lambda^{1/T_n}}$$

It is easy to check that Δ_n is a bound for the probability of accepting a death obtained by reversing (8). Under smooth assumptions we have

$$1 \geq \min\left\{1, \frac{p_b n(\mathbf{y}+1)}{p_d \nu(K)} \frac{p_n(\mathbf{y} \setminus \{\eta\})}{p_n(\mathbf{y})}\right\} \geq \frac{p_b}{p_d \nu(K)} \frac{1}{\Lambda^{1/T_n}}$$

From the relation (19), we obtain

$$P_n^\delta(\mathbf{y}, A) \geq (pb\Delta_n)^\delta \lambda_{\Xi_0}(A) \tag{20}$$

where λ_{Ξ_0} is the function defined as follows :

$$\lambda_{\Xi_0}(A) = \begin{cases} 1 & \text{if} \quad A = \Xi_0 \\ 0 & \text{elsewhere} \end{cases}$$

Similarly, from the relation (19), we obtain

$$P_n^\delta(\mathbf{y}, A) \leq 1 - (p_b \Delta_n)^\delta \lambda_{\Omega \setminus \Xi_0}(A) \tag{21}$$

with $\lambda_{\Omega \setminus \Xi_0}$ being a function such that:

$$\lambda_{\Omega \setminus \Xi_0}(A) = \begin{cases} 1 & \text{if} \quad A \subseteq \Omega \setminus \Xi_0 \\ 0 & \text{elsewhere} \end{cases}$$

By grouping together the equations (20) and (21) we obtain:

$$|P_n^\delta(\mathbf{x}, A) - P_n^\delta(\mathbf{y}, A)| \leq 1 - (p_b \Delta_n)^\delta [\lambda_{\Xi_0}(A) + \lambda_{\Omega \setminus \Xi_0}(A)] \tag{22}$$

Clearly, for $A = \Xi_0$ or $A \subseteq \Omega \setminus \Xi_0$ the inequality (22) becomes

$$|P_n^\delta(\mathbf{x}, A) - P_n^\delta(\mathbf{y}, A)| \leq 1 - (p_b \Delta_n)^\delta \tag{23}$$

If $A = \Xi_0 \cup A_1$ with $A_1 \subseteq \Omega \setminus \Xi_0$, we have:

$$\begin{aligned} & P_n^\delta(\mathbf{x}, A) = \\ & = P_n^\delta(\mathbf{x}, \Xi_0) + P_n^\delta(\mathbf{x}, A_1) \\ & = P_n^\delta(\mathbf{x}, \Xi_0) + 1 - P_n^\delta(\mathbf{x}, \Xi_0) - P_n^\delta(\mathbf{x}, \Omega \setminus \Xi_0 \setminus A_1) \\ & = 1 - P_n^\delta(\mathbf{x}, B) \end{aligned}$$

with $B = (\Omega \setminus \Xi_0 \setminus A_1) \subseteq (\Omega \setminus \Xi_0)$. In this case, the inequality (23) is still fulfilled :

$$|P_n^\delta(\mathbf{x}, A) - P_n^\delta(\mathbf{y}, A)| = |P_n^\delta(\mathbf{y}, B) - P_n^\delta(\mathbf{x}, B)| \leq 1 - (p_b \Delta_n)^\delta \tag{24}$$

Therefore, replacing the inequalities (23) and (24) in (15), we obtain for the Dobrushin coefficient

$$c(Q_n) \leq 1 - (p_b \Delta_n)^\delta$$

Obviously, a cooling schedule can be found if

$$\left(\frac{p_b}{\nu(K) \Lambda^{1/T_n}} \right)^\delta \geq \frac{1}{n}$$

that gives, under mild conditions,

$$T_n \geq \frac{\delta \log \Lambda}{\log(n) + \delta \log \frac{p_b}{\nu(K)}}$$

whenever $n \to \infty$.

□

4.3 Simulation study and discussion

In this section, we show examples of patterns constructed by sampling the Bisous model.

The Metropolis-Hastings dynamics used to simulate the model, has for the transition kernel the following parameters $p_b = 0.4$,$p_d = 0.3$ and $p_c = 0.3$. All the simulations were ran starting with the empty configuration.

Concerning the simulated annealing, a good choice of the initial temperature $T_0 = \delta \log \Lambda$ is crucial. If the algorithm is started with a too small initial temperature, it may get "frozen" in a local optimum. Still, in practice it is often the case that a compromise has to be found since the theoretical value of T_0 may be rather high [4].

This problem cannot be avoided in this case, neither. Clearly, we have a bound for the local stability constant (6). The conditions of Theorem 4 are easily respected if hard-core interactions are considered between the objects forming a pattern. If such conditions are not suitable for the problem on hand, the configuration state space may be truncated, if prior knowledge with respect the number of objects in a pattern, is available. Hence, we can easily compute values of δ and $\log \Lambda$ satisfying the convergence properties of the simulated annealing algorithm. But like in the finite state space case, the cooling schedule is slow from a practical point of view. These reasons made us voting for the approximation of the cooling schedule:

$$T_n = \frac{1}{\log(n+1)} \tag{25}$$

with the parameters values $\delta = 1000$ and $\Lambda = 0.001$.

The simulated annealing algorithm was implemented using the Metropolis-Hastings dynamics that has the parameters mentioned previously. As indicated by the Theorem 4, the temperature is lowered using (25) every δ steps.

Example 1. Line pattern (continued). *The model was simulated in a three dimensional window,* $K = [0, 100] \times [0, 100] \times [0, 100]$. *The parameters of the object presented in Figure 1 are* $r = 5.0$ *and* $r_a = 0.5$. *The* τ *parameter for the alignment is 0.125. The soft repulsion is combined with alignment in such a way that, configurations made of objects that are separated by a distance smaller than* r_s *and that are not well aligned will be penalized.*

The connectivity parameters of the Bisous model density (5) are $\gamma_0 = 0.001$, $\gamma_1 = 0.1$, $\gamma_2 = 5.0$, *and the pairwise interaction parameters are* $\gamma_h = 0$ *and the penalization parameter for the soft-core repulsion combined with bad alignment is* $\gamma_{r,\|} = 0.1$.

The presented Metropolis-Hastings dynamics was run for 10^7 *iterations, whereas the simulated annealing algorithm was run for* 5×10^7 *iterations. The results of simulation are shown in Figure 4 and Figure 5. The spherical representation of the pattern is obtained drawing around the center of each object, the sphere designing the hard-core repulsion, whereas the segment representation was obtained plotting for each object the segment formed by its corresponding* $q = 2$ *extremity points. Sufficient statistics were observed every* 10^3 *steps, within a window* $W = [20, 80] \times [20, 80] \times [20, 80]$ *in order to prevent bias [2].*

The pattern obtained simulating the Bisous model of the given parameteres, when using a Metropolis-Hastings dynamics, tends to connect segments but it has quite a random structure. We can notice that, when the temperature is lowered, i.e. running the simulated annealing algorithm, the segments are getting connected much more often forming filaments.

Example 2. Planar pattern (continued). *The object presented in Figure 2 has the same geometrical parameters and the same pairwise intercations like in the previous example. The main difference comes as explained earlier, from the number of possible connections* $q = 6$ *and the pre-defined attraction rule* $\mathcal{C}$*.*

The connectivity parameters of the employed probability density (5) are $\gamma_0 = 0.001$*,* $\gamma_1 = 0.15$*,* $\gamma_2 = 0.3$*,* $\gamma_3 = 0.9$*,* $\gamma_4 = 1.5$*,* $\gamma_5 = \gamma_6 = 5.0$ *and the pairwise interaction parameters are* $\gamma_h = 0$ *and* $\gamma_{r,\|} = 0.1$*. The model was simulated in a three dimensional window,* $K = [0, 100] \times [0, 100] \times [0, 100]$*.*

The number of iterations for the algorithms, the spacing for taking the samples, and the size of the observing window were exactly the ones used for the line pattern case. The results of simulation are shown in Figure 6 and Figure 7. The polygonal representation is obtained drawing around the centre of each object the hexagone formed by its extremity points.

For the given parameters, the pattern obtained with Metropolis-Hastings do not connect too many hexagones in order to form planar structures. Still, when the temperature is lowered, obvious surfaces structures are formed.

Example 3. Cluster pattern (continued). *The object represented in Figure 3 was used to simulate clustered patterns. The same geometrical parameters and pairwise interactions were used as in the previous cases. The difference consists of the number of extremity points to be connected* $q = 12$ *and the associated attraction rule.*

The connectivity parameters of the sampled probability density (5) are $\gamma_0 = 0.001$*,* $\gamma_1 = 0.15$*,* $\gamma_2 = 0.3$*,* $\gamma_3 = 0.9$*,* $\gamma_4 = 1.5$*,* $\gamma_s = 5.0$ *with* $s =$

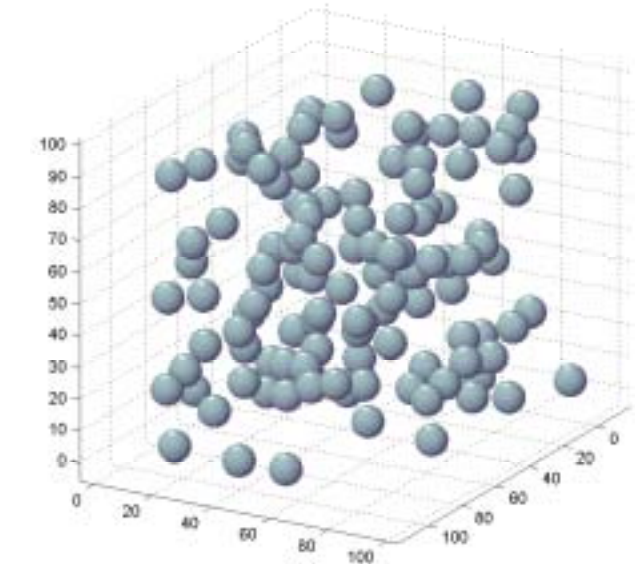

Figure 4: Line pattern obtained by sampling Bisous model with a Metropolis-Hastings dynamics : a) spherical representation, b) segment representation, c) the evolution of the total number of objects in the pattern, d)$\bar{n}_t = 31.60$ cumulative mean of the total number of objects in a configuration

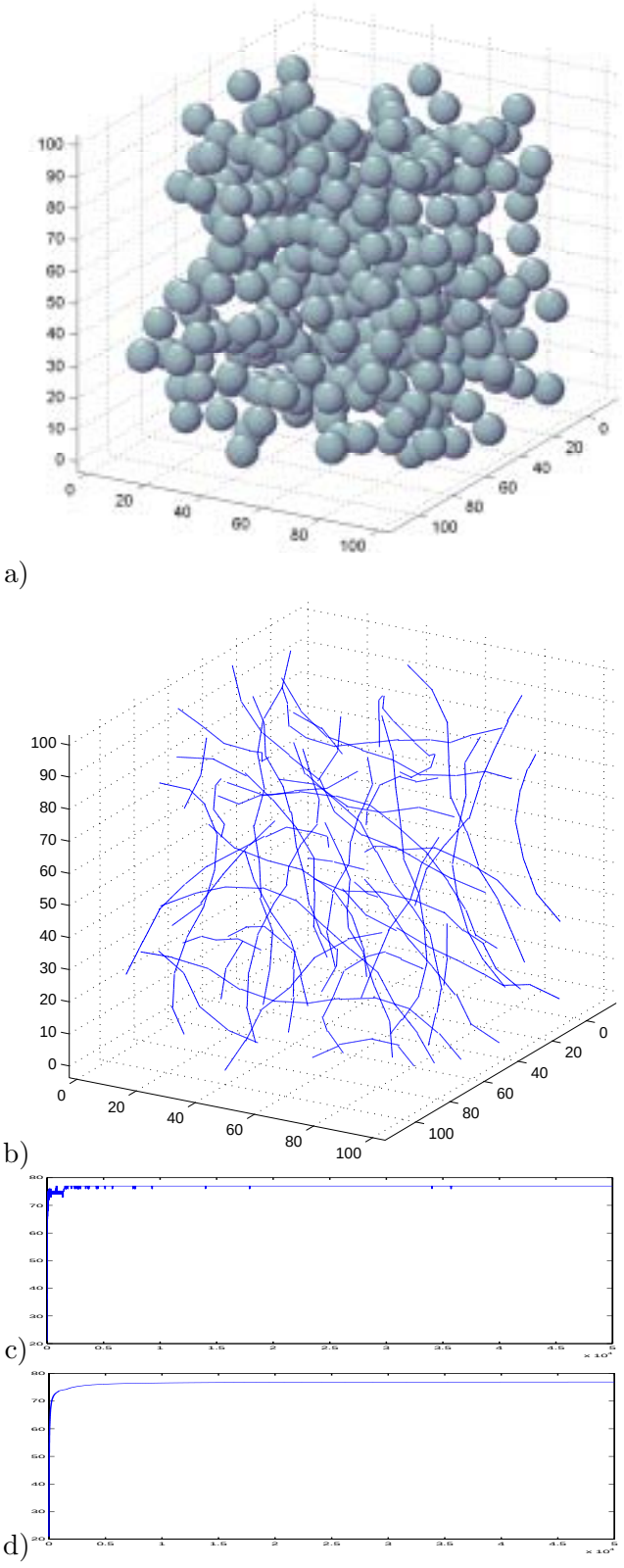

Figure 5: Line pattern obtained by sampling Bisous model with a simulated annealing algorithm : a) spherical representation, b) segment representation, c) the evolution of the total number of objects in the pattern, d) $\bar{n}_t = 76.91$ cumulative mean of the total number of objects in a configuration

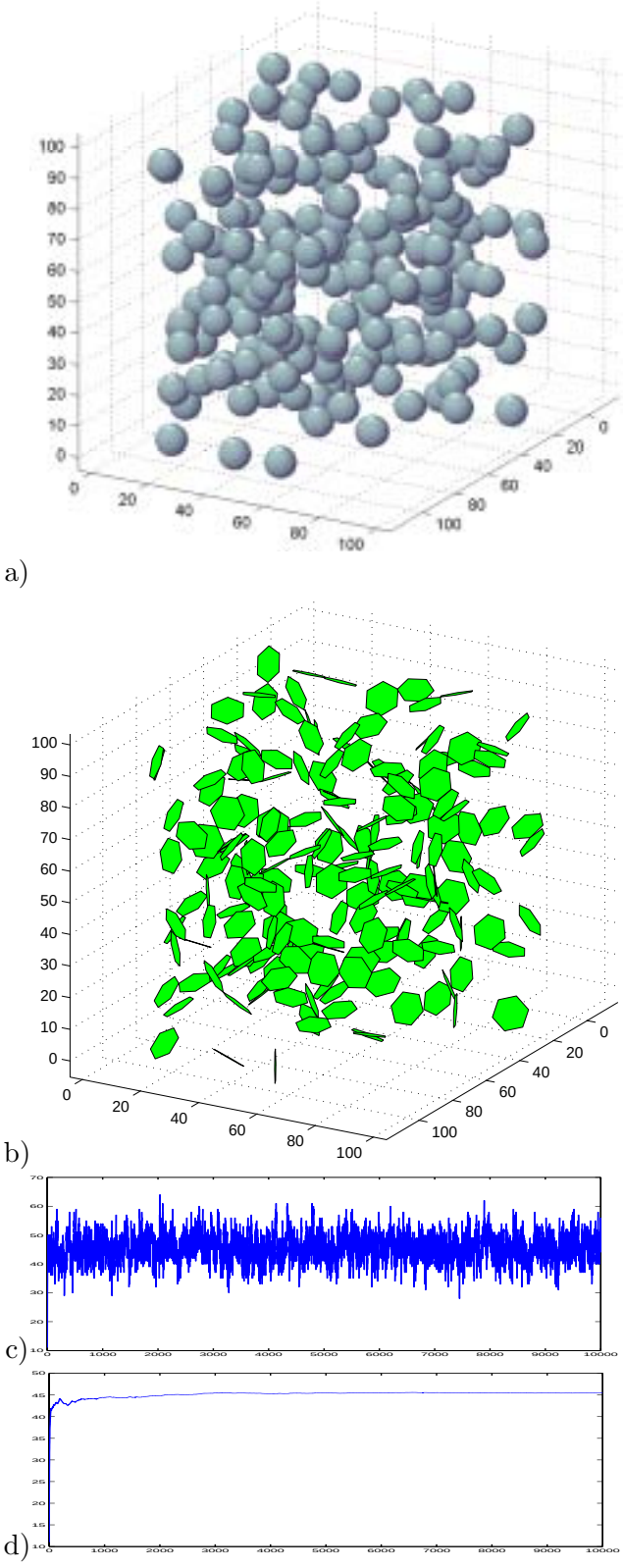

Figure 6: Planar pattern obtained by sampling Bisous model with a Metropolis-Hastings dynamics : a) spherical representation, b) polygonal representation, c) the evolution of the total number of objects in the pattern, d) $\bar{n}_t = 45.49$ cumulative mean of the total number of objects in a configuration

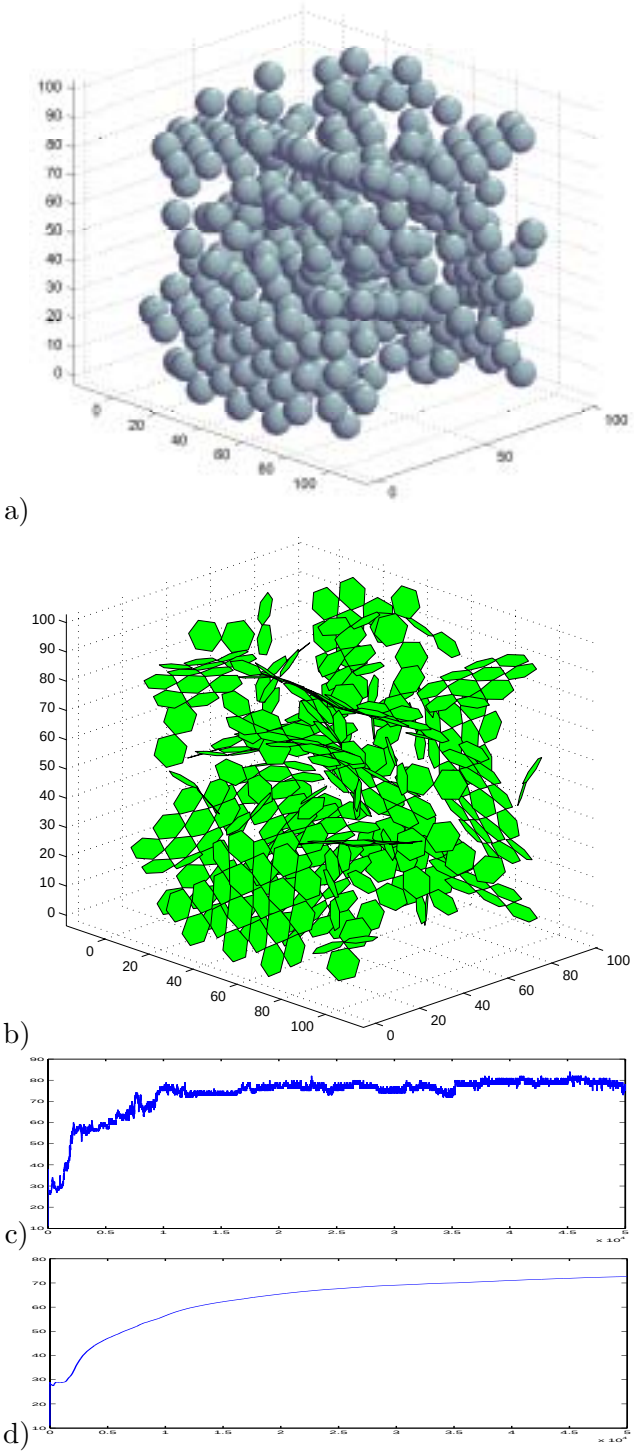

Figure 7: Planar pattern obtained by sampling Bisous model with a simulated annealing algorithm : a) spherical representation, b) polygonal representation, c) the evolution of the total number of objects in the pattern, d) $\bar{n}_t = 72.63$ cumulative mean of the total number of objects in a configuration

$5, \ldots, 12$. *The pairwise interaction parameters as well as the size of the sampling window are the same as in the previous two examples.*

The number of iterations for the algorithms, the spacing for taking the samples, and the size of the observing window remain unchanged. The results of simulation are shown in Figure 8 and Figure 9. The polyhedral representation is obtained drawing around the centre of each object the cuboctahedron formed by its extremity points.

For the given parameters, the pattern obtained with Metropolis-Hastings do not connect too many polyhedra in order to form clustered structures. Still, when the temperature is lowered, obvious clustered volume structures are formed.

The parameters chosen for the previous examples were fixed in order to favour the connectivity among the objects. Patterns with different topologies may be obtained for instance, if a higher curvature for the alignment between objects is allowed or different weights are given to the model parameters related to the connectivity.

It is possible to sample from the Bisous model in order to obtain complex geometrical shapes using only the Metropolis-Hastings algorithm. In this case, the ratio between the parameters allowing high connectivity and the ones penalizing free objects or less connected ones, will be really high. This phenomenon becomes more important when planar or cluster patterns are simulated : the high connected objects appear in a configuration via the less connected ones. This may indicate also the limits of the Metropolis-Hastings dynamics. Clearly the strong point of the proposed dynamics consists of its tailored moves, but on the other hand, it acts at only one object at the time.

In this sense, the simulated annealing overcomes the drawback of the Metropolis-Hastings dynamics. At high temperatures the undesired configurations, in this case the less connected patterns, are allowed. While the temperature decreases, the free or the less connected objects are frozen and the connected patterns are formed. We can notice this phenomenon from the evolution of the sufficient statistics : their behaviour becomes less "random" at low temperatures, in the sense that only the objects increasing the energy of the system tend to be accepted in the configuration.

We would like to reinforce, that the simulated annealing is not a sampling method from a un-normalized probability density. When convergence is reached it can be seen as a sampling method over the sub-space of configurations maximizing the probability density of interest. Hence, when used for spatial pattern analysis, running a simulated annealing algorithm over $p(\mathbf{y})$ indicates if the prior we have chosen is appropriate for the problem on

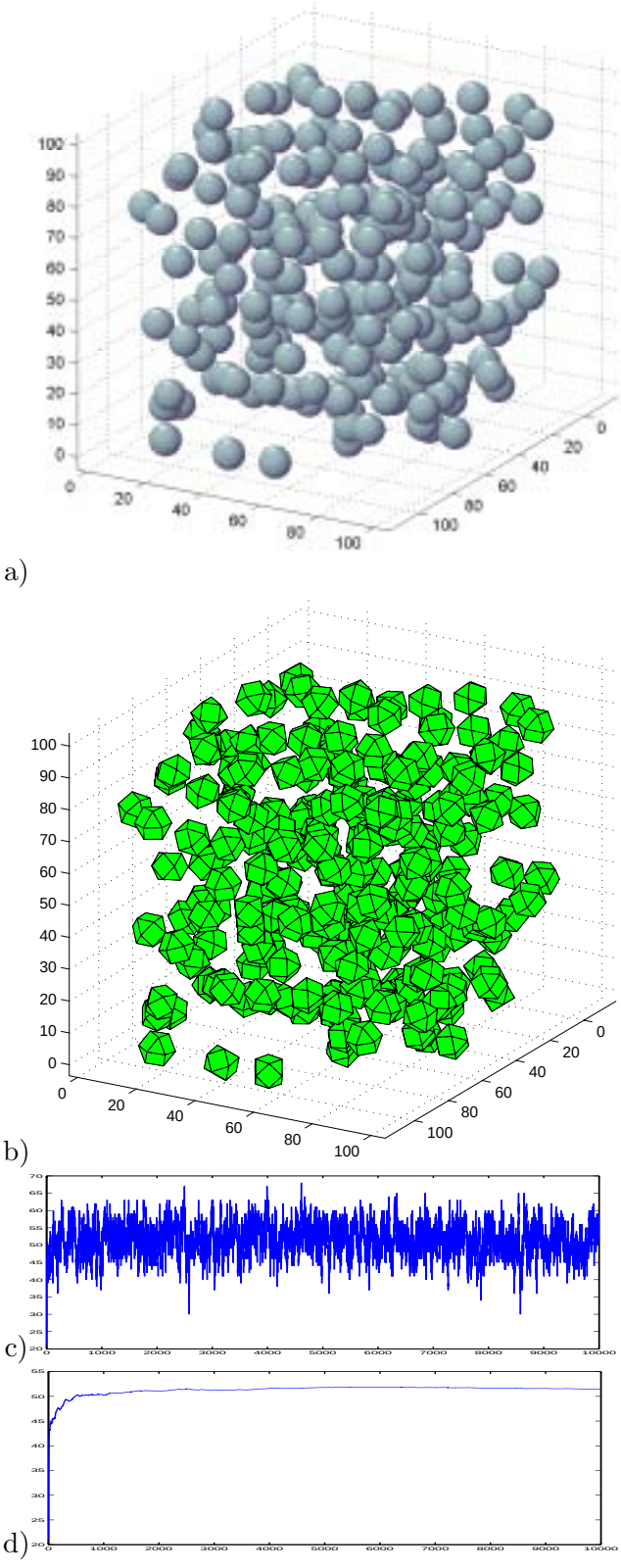

Figure 8: Cluster pattern obtained by sampling Bisous model with a Metropolis-Hastings dynamics : a) spherical representation, b) polyhedral representation, c) the evolution of the total number of objects in the pattern, d) $\bar{n}_t = 51.49$ cumulative mean of the total number of objects in a configuration

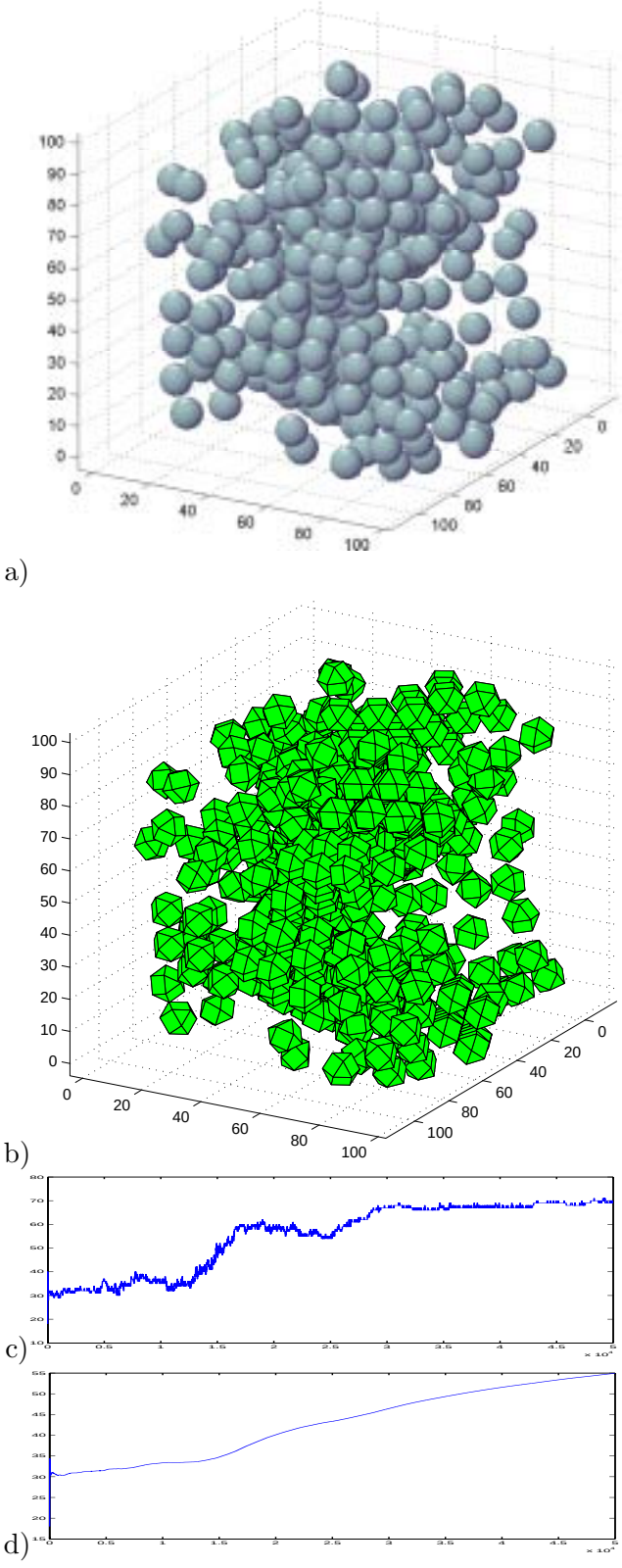

Figure 9: Cluster pattern obtained by sampling Bisous model with a simulated annealing algorithm : a) spherical representation, b) polyhedral representation, c) the evolution of the total number of objects in the pattern, d) $\bar{n}_t = 54.93$ cumulative mean of the total number of objects in a configuration

hand. The complete solution, for instance the pattern extracted from the data to be analyzed, is obtained only after adding to the prior density the conditional probability density or the external field related to the data, in order to form the likelihood function.

The convergence result presented in Theorem 4 is the first one of this type related to the simulated annealing based on Metropolis-Hastings dynamics applied to marked point processes. The result obtained by [16] stands only for spatial birth-and-death processes. This simulation dynamics requires a low value of the local stability constant of the point process of interest and allows only uniform proposals for adding and deleting an object from the configuration. The Metropolis-Hastings dynamics requires just the local stability and allows adapted transition kernels. Furthermore, the practical results presented in [16] are obtained running a simulated annealing algorithm at low fixed temperature.

In physics, when large number of objects are involved, speeding-up strategies are studied for the application of the simulated annealing when finding minimal energy states for systems containing a fixed number of hard spheres [14]. This may be an interesting direction to observe when simulating marked point processes. Still, these new strategies do not preserve always the detailed balance. Hence in this case, the statistical inference performed when sampling at fixed temperature is not effective.

For computational reasons, we had to approximate our cooling schedule. Even in this case, our algorithm respects the detailed balance and the key principle of the simulated annealing algorithms that intents to not get stuck in local minima, *i.e.* starting with configurations at high temperatures and sampling from the distribution of interest while cooling slowly the temperature.

5 Conclusion and perspectives

In this paper, we have presented an object point process - Bisous model - able to simulate random patterns exhibiting a complex geometry, that are made of simple interacting objects. The topology of the configurations is controled via the choice of the generating element or via the model parameters. We consider these results not only a three dimensions extention of the work in [18, 33]. The Bisous model is an open structure that gives a considerable freedom in choosing attraction rules, shape and type of the generating elements, hence allowing the modelling of a wide range of patterns.

The simulation of such a model is done using Monte Carlo methods.

To this purpose, a tailored Metropolis-Hastings dynamics and a simulated annealing algorithm were proposed. Theoretical properties of the model and of the simulation methods were investigated.

The immediate motivation of introducing such a model was given by a practical application in astronomy. Galaxies are seldom isolated. They are usually found in groups or clusters, beeing a part of larger structures. Arranged in interconnected walls or fillaments, galaxies form a cosmic web that surrounds almost empty regions [20]. Recently, two dimensional simulated astronomical data was analysed using the Candy model [35]. Actually, we have all the necessary ingredients to tackle the problem of studying the distribution of galaxies using real three dimensional data.

The Bisous model can be adapted in order to be used for other practical applications like studying blood vessels or fractures network for medical image analysis or geological purposes, respectively. In physics, polymer or protein structures as well as liquid crystals exhibit complex geometrical shapes, that may suggest the use of models that are similar to the one presented in this paper. Studying packing densities having Bisous model as a starting point is, in our opinion, another open question [21].

These practical applications will require theoretical modifications with respect the modelling. Interactions between objects of different types as well as inhomogeneity has to be considered [8].

At current status, the results obtained are under the question of convergence diagnosis. The stationarity showed by the curve of the sufficient statistics obtained using the Metropolis-Hastings does not indicate the convergence. The same statement holds for the simulated annealing. Perfect simulation for marked point processes is still an open problem [19]. Recently developed techniques like the perfect simulated tempering [23], may indicate the direction for further investigation to be done with respect the simulation of the Bisous model.

References

[1] A. J. Baddeley and M. N. M. van Lieshout. Stochastic geometry models in high-level vision. In K. V. Mardia and G. K. Kanji, editors, *Statistics and Images Volume 1, Advances in Applied Statistics, a supplement to Journal of Applied Statistics*, 20:231–256, Abingdon, 1993, Carfax.

[2] A. J. Baddeley. Spatial sampling and censoring, in: O. Barndorff-Nielsen, W. S. Kendall and M. N. M. van Lieshout (eds.), *Stochastic*

geometry, likelihood and computation, CRC Press/Chapman and Hall, Boca Raton, 1999.

[3] X. Descombes, R. S. Stoica, L. Garcin and J. Zerubia. A RJMCMC algorithm for object processes in image processing. *Monte Carlo Methods and Applications*, 7 : 149–156, 2001.

[4] S. Geman and D. Geman. Stochastic relaxation, Gibbs distribution and Bayesian restoration of images. *IEEE Transactions on Pattern Analysis and Machine Inteligence*, 6 : 721–741, 1984.

[5] C.J. Geyer and J. Møller. Simulation procedures and likelihood inference for spatial point processes. *Scandinavian Journal of Statistics*, 21:359–373, 1994.

[6] C. J. Geyer. Likelihood inference for spatial point processes, in: O. Barndorff-Nielsen, W. S. Kendall and M. N. M. van Lieshout (eds.), *Stochastic geometry, likelihood and computation*, CRC Press/Chapman and Hall, Boca Raton, 1999.

[7] P.J. Green. Reversible jump MCMC computation and Bayesian model determination. *Biometrika*, 82:711-732, 1995.

[8] U. Hahn, E. B. V. Jensen, M. N. M. van Lieshout and L. S. Nielsen. Inhomogeneous spatial point processes by location dependent scaling. *Advances in Applied Probability (SGSA)*, 35 : 319–336, 2003.

[9] B. Hajek. Cooling schedules for optimal annealing. *Mathematics of Operation Research*, 13(2):311–329, 1988.

[10] M.B. Hansen, J. Møller and F.Aa. Tøgersen. Bayesian contour detection in a time series of ultrasound images through dynamic deformable template models. *Biostatistics*, 3:213–228,2002.

[11] D. Hearn and M. P. Baker *Computer Graphics. Second Edition.* Prentice-Hall, Englewood Cliffs, NJ, 1994.

[12] W. S. Kendall and J. Møller. Perfect simulation using dominating processes on ordered spaces, with application to locally stable point processes. *Advances in Applied Probability (SGSA)*, 32:844–865, 2000.

[13] S. Kirkpatrick, G. D. Gellat Jr. and M. P. Vecchi. Optimization by simulated annealing. *Science*, 220 : 671–680, 1983.

[14] J. Klos and S. Kobe. Simulated annealing with Tsallis weights for a system of interacting hard spheres. *Journal of Physics A : Mathematical and General*, 35 : 6261–6269, 2002.

[15] C. Lacoste, X. Descombes and J. Zerubia. A comparative ctudy of point processes for line network extraction in remote sensing. *Research report No. 4516*, INRIA Sophia-Antipolis, 2002.

[16] M. N. M. van Lieshout. Stochastic annealing for nearest-neighbour point processes with application to object recognition. *Advances in Applied Probability*, 26 : 281 –300, 1994.

[17] M .N. M. van Lieshout. *Markov point processes and their applications*. London/Singapore: Imperial College Press/World Scientific Publishing, 2000.

[18] M. N. M. van Lieshout and R. S. Stoica. The Candy model revisited: properties and inference. *Statistica Neerlandica*, 57:1–30, 2003.

[19] M. N. M. van Lieshout and R. S. Stoica. Perfect simulation for marked point processes. *CWI Research Report* PNA-0306, 2003.

[20] V. J. Martinez and E. Saar. *Statistics of the galaxy distribution*. Chapman & Hall/CRC, 2002.

[21] S. Mase, J. Møller, D. Stoyan, R.P. Waagepetersen and G. Döge. Packing densities and simulated tempering for hard core Gibbs point processes. *Annals of the Institute of Statistical* Mathematics, 53 : 661 - 680, 2001.

[22] S. P. Meyn and R. L. Tweedie. *Markov chains and stochastic stability*. Springer-Verlag, London, 1993.

[23] J. Møller and G. Nicholls. Perfect simulation for sample-based inference. *Research Report R-99-2011*, Department of Mathematical Sciences, Aalborg University, 1999. To appear in *Statistics and Computing*.

[24] M. Ortner, X. Descombes and J. Zerubia. Building extraction from digital elevation model. *Research report No. 4517*, INRIA Sophia Antipolis, 2002.

[25] A. Pievatolo and P. J. Green. Boundary detection through dynamic polygons. *Journal of the Royal Statistical Society, Series B*, 60 : 609–626,1998.

[26] C.J. Preston. Spatial birth-and-death processes. *Bulletin of the International Statistical Institute*, 46:371–391, 1977.

[27] R. -D. Reiss. *A course on point processes*, Springer-Verlag, New York, 1993.

[28] B.D. Ripley and F.P. Kelly. Markov point processes. *Journal of the London Mathematical Society*, 15:188–192, 1977.

[29] H. Rue and O. K. Husby. Identification of Partly Destroyed Objects using Deformable Templates. *Statistics and Computing*, 8 : 221–228, 1998.

[30] H. Rue and A. R. Syversveen. Bayesian object recognition with Baddeley's Delta loss. *Advances in Applied Probability (SGSA)*, 30 : 64–84, 1998.

[31] H. Rue and M. Hurn. Bayesian object identification. *Biometrika*, 3 : 649–660, 1999.

[32] D. Ruelle. *Statistical mechanics*. Wiley, New York, 1969.

[33] R. S. Stoica. *Processus ponctuels pour l'extraction des réseaux linéiques dans les images satellitaires et aériennes*. PhD Thesis (in French), Nice Sophia-Antipolis University, 2001.

[34] R. S. Stoica, X. Descombes and J. Zerubia. A Gibbs point process for road extraction in remotely sensed images. *International Journal of Computer Vision*, 57(2):121–136, 2004.

[35] R. S. Stoica, V. J. Martinez, J. Mateu and E. Saar. Detection of cosmic filaments using the Candy model. *Research report n.68-2004*, University Jaume I Castellon, 2004.

[36] L. Tierney. Markov chains for exploring posterior distributions. *Annals of Statistics*, 22:1701–1728, 1994.